Neuron, Vol. 42, 9–21, April 8, 2004, Copyright ©2004 by Cell Press

In Vivo Imaging of Neuronal Activity by Targeted Expression of a Genetically Encoded Probe in the Mouse

Neurotechnique

Thomas Bozza,[2,3] John P. McGann,[1,3] Peter Mombaerts,[2] and Matt Wachowiak[1,*]
[1]Department of Biology
Boston University
Boston, Massachusetts 02215
[2]The Rockefeller University
New York, New York 10021

Summary

Genetically encoded probes show great promise in permitting functional imaging of specified neuronal populations in the intact nervous system, yet their in vivo application has been limited. Here, we have targeted expression of synapto-pHluorin, a pH-sensitive protein that reports synaptic vesicle fusion, to olfactory sensory neurons in mouse. Synapto-pHluorin selectively labeled presynaptic terminals of sensory neurons in glomeruli of the olfactory bulb. Odorant stimulation evoked large-amplitude fluorescence increases that were localized to individual glomeruli in vivo, correlated with presynaptic calcium influx, graded with stimulus intensity, and stable over a period of days. Spatial patterns of odorant-activated glomeruli were distributed and did not change systematically with increasing carbon chain length, in contrast to the finely organized chemotopy that has been reported using other imaging methods. Targeted expression of synapto-pHluorin in mouse will permit the analysis of previously inaccessible neuronal populations and chronic imaging from genetically identified neurons in vivo.

Introduction

Methods for monitoring the activity of defined neuronal populations in intact animals contribute greatly to our understanding of nervous system function in vertebrates. Optical imaging using conventional fluorescent dyes allows physiological changes to be recorded in many individual neurons simultaneously (reviewed by Djurisic et al., 2003). However, the need to introduce exogenous dyes into neuronal tissues often limits applications of this approach. Dye application is necessarily invasive. Dyes may stain neuronal and nonneuronal cells indiscriminately, may produce varied labeling, or may fail to label certain neurons altogether. Dyes are also cleared from tissues, preventing chronic imaging in intact animals.

In view of these limitations, genetically encoded, protein-based indicators have great potential for monitoring neuronal activity in vivo (Miyawaki, 2003). Such probes can be targeted for expression in specific neuronal populations or cellular compartments. Specificity of targeting is limited only by patterns of gene expression. The probe is constantly produced and permanently labels neurons, affording the opportunity for long-term, selective imaging.

Despite this promise, the use of genetically encoded probes for monitoring neuronal activity in intact animals has been limited. Probes that are potentially useful for such studies include fluorescent indicators of voltage (Siegel and Isacoff, 1997; Sakai et al., 2001; Ataka and Pieribone, 2002), calcium (Romoser et al., 1997; Baird et al., 1999; Nagai et al., 2001; Nakai et al., 2001; Truong et al., 2001), chloride (Kuner and Augustine, 2000), or neurotransmitter release (Miesenböck et al., 1998). Voltage-sensitive probes have been characterized in cultured cells and oocytes (Siegel and Isacoff, 1997; Sakai et al., 2001; Ataka and Pieribone, 2002) but have not been used in more complex systems. Indicators for calcium (cameleons, camgaroos, pericams, and G-CaMP) have been effective in vitro, in intact invertebrates (Kerr et al., 2000; Fiala et al., 2002; Wang et al., 2003; Yu et al., 2003) and zebrafish (Higashijima et al., 2003). The signals produced by the calcium indicators are relatively small compared with their chemical counterparts and display decreased dynamic ranges when expressed in transgenic animals as compared with transient expression in vitro (Miyawaki, 2003). These probes have not been successfully used in mammalian models.

Here, we show that an indicator of neurotransmitter release, synapto-pHluorin (spH), reports neuronal activity when targeted to mature olfactory sensory neurons (OSNs) in mice. SpH is a fusion of a pH-sensitive green fluorescent protein variant (ecliptic pHluorin) with the mouse synaptic vesicle-associated protein VAMP-2 (Miesenböck et al., 1998). The fluorescent domain is localized to the acidic lumen of presynaptic vesicles where it is ~20-fold less fluorescent than at neutral pH (Sankaranarayanan et al., 2000). During vesicle fusion, the vesicle lumen becomes continuous with the extracellular space, resulting in an increase in pH and an increase in fluorescence (Miesenböck et al., 1998). Action potential firing in spH-expressing neurons thus drives fluorescence increases in their presynaptic terminals. Selective expression of spH in the fly antennal lobe has permitted functional imaging of olfactory circuitry in *Drosophila* (Ng et al., 2002).

We used spH to monitor odorant-evoked activation of mouse OSNs. These neurons line the nasal cavity where they detect odorants via odorant receptor proteins expressed on their cell surface. Each OSN projects one axon to the olfactory bulb where it synapses in a glomerulus. Olfactory glomeruli represent sites of convergence of axons from OSNs that express the same odorant receptor (Mombaerts, 1999) and share similar odorant response profiles (Bozza et al., 2002). In addition to receiving highly convergent, anatomically and functionally distinct inputs, glomeruli are optically accessible in vivo, making them excellent targets for imaging neuronal activity.

We generated a strain of mice expressing spH in all mature OSNs, resulting in the selective labeling of their terminals in olfactory glomeruli. Odorant stimulation evoked graded fluorescence increases in odorant-spe-

*Correspondence: dmattw@bu.edu
[3]These authors contributed equally to this work.

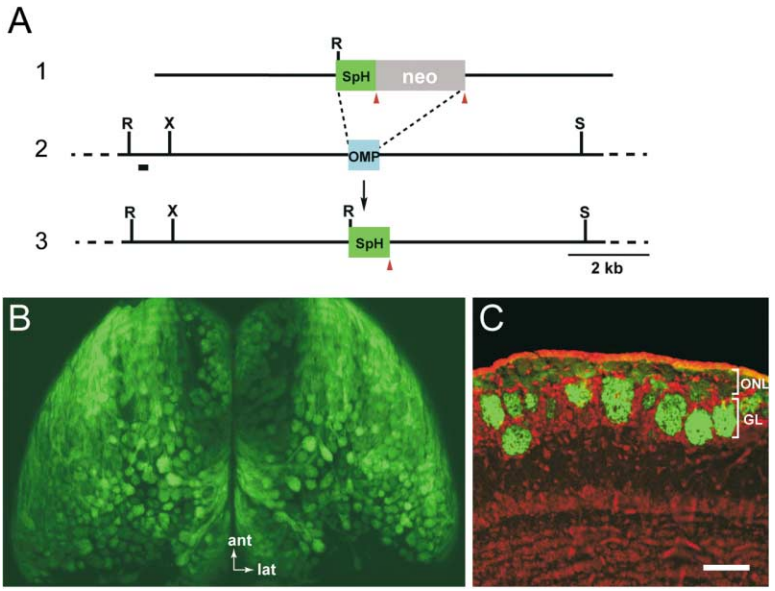

Figure 1. Targeting SpH to Olfactory Sensory Neurons

(A) Diagram of the *OMP* targeting vector (1). The coding sequence for superecliptic synapto-pHluorin (green box; spH) replaces the *OMP* coding sequence (blue box, OMP) shown in the wild-type locus (2). The autoexcising *neomycin* selectable marker (gray box, neo) is flanked by *loxP* sites (red arrowheads). Following homologous recombination and passage through the germline, the selectable cassette is removed, leaving the *spH* coding sequence followed by a single *loxP* site (3). Black box indicates the probe used to screen for homologous recombinants. Relevant restriction sites are shown (RI, EcoRI; X, XhoI; S, SphI).

(B) Whole-mount view of the left and right dorsal olfactory bulbs from a homozygous OMP-spH mouse using confocal fluorescence microscopy. SpH labels glomeruli (round structures) and axon bundles which cover the surface of the bulbs. Anterior (ant) and lateral (lat) are indicated.

(C) Section through the olfactory bulb from a homozygous OMP-spH mouse showing preferential labeling in the glomerular layer (GL) and less intense labeling of the overlying olfactory nerve layer (ONL). The section is counterstained with the nuclear dye TOTO-3 (red). Scale bar, 400 μm in (B); 100 μm in (C).

cific patterns of glomeruli that correspond to glomeruli exhibiting presynaptic calcium influx. SpH expression and odorant-evoked signals were stable, permitting chronic imaging of neuronal activity. Finally, we exploited the fidelity and spatial resolution of the spH signal to investigate relationships between spatial patterns of glomerular activity and odorant chemical structure.

Results

Targeted Expression of SpH

By gene targeting in embryonic stem cells, we created a mouse strain in which spH is expressed from the locus encoding the olfactory marker protein (OMP) (Figure 1A). OMP is selectively and highly expressed in mature OSNs, and this locus has been used previously to express histological markers such as tau-lacZ (Mombaerts et al., 1996) and GFP (Potter et al., 2001). In OMP-synapto-pHluorin (OMP-spH) mice, green fluorescence is seen in glomeruli of the olfactory bulb, with less-intense fluorescence in the superficial nerve layer containing the axons of OSNs (Figures 1B and 1C). This distribution is consistent with enrichment of spH in presynaptic terminals. While spH within the lumen of synaptic vesicles is practically nonfluorescent (Miesenböck et al., 1998), fluorescence in the absence of stimulus-induced activity (resting fluorescence) is consistent with previous studies showing a small (~10%) but highly fluorescent fraction of spH protein localized to the plasma membrane (Sankaranarayanan et al., 2000). Resting fluorescence may also reflect spontaneous activity of OSNs.

In OMP-spH mice, all glomeruli appear labeled but with variable intensity (Figure 1B). Fluorescence intensity did not correlate with glomerular area measured in unfixed whole mounts using confocal microscopy ($r = 0.05$, $df = 102$, $p = 0.63$, one mouse). The variability persisted in pH-neutralized preparations (data not shown). This variability is unlikely to result from variation in glomerular size or differences in the fraction of spH on the plasma membrane but instead may reflect variation in OMP expression across OSN populations.

SpH Signals Report OSN Input to Olfactory Bulb Glomeruli

SpH-labeled glomeruli on the dorsal surface of the olfactory bulb are visible through thinned bone in vivo (Figure 2A). We measured odorant-evoked optical signals from the dorsal bulb in 28 OMP-spH mice using methods established for imaging calcium-sensitive dye signals from glomeruli (Wachowiak and Cohen, 2001). In all mice, odorants elicited focal increases in fluorescence (Figures 2B and 2D). We detected no focal fluorescence decreases nor did we detect fluorescence changes in the absence of odorant stimulation (except photobleaching, see below). Discrete foci in the response maps were often associated with glomeruli discernable in the resting fluorescence images (Figures 2E and 2F).

The diameter of the signal foci (93.1 ± 2.9 μm, $n = 52$ glomeruli) was indistinguishable from that of individual glomeruli measured from whole-mount confocal images (93.5 ± 2.2 μm, $n = 104$ glomeruli; t test, $df = 154$, $p = 0.35$). Thus, focal spH signals reflect the activation of individual glomeruli. The resolution of spH response patterns was such that profiles of adjacent activated glomeruli were visible and distinct (Figures 2E and 2F).

The odorant-evoked spH signal was superimposed on a continuous, exponentially decaying fluorescence decrease resulting from photobleaching (mean time constant, 3.1 ± 0.3 s, $n = 7$ preparations) (Figure 2G). Typical 10 s trials caused a decrease in the average resting fluorescence of $6.6\% \pm 0.2\%$ ($n = 7$; from no-odor trials). We corrected for photobleaching in stimulus trials by subtracting a no-odor trial before further analysis (Figures 2G and 2H). Surprisingly, resting fluorescence levels recovered spontaneously and rapidly from bleaching, such that a 90 s recovery period was suffi-

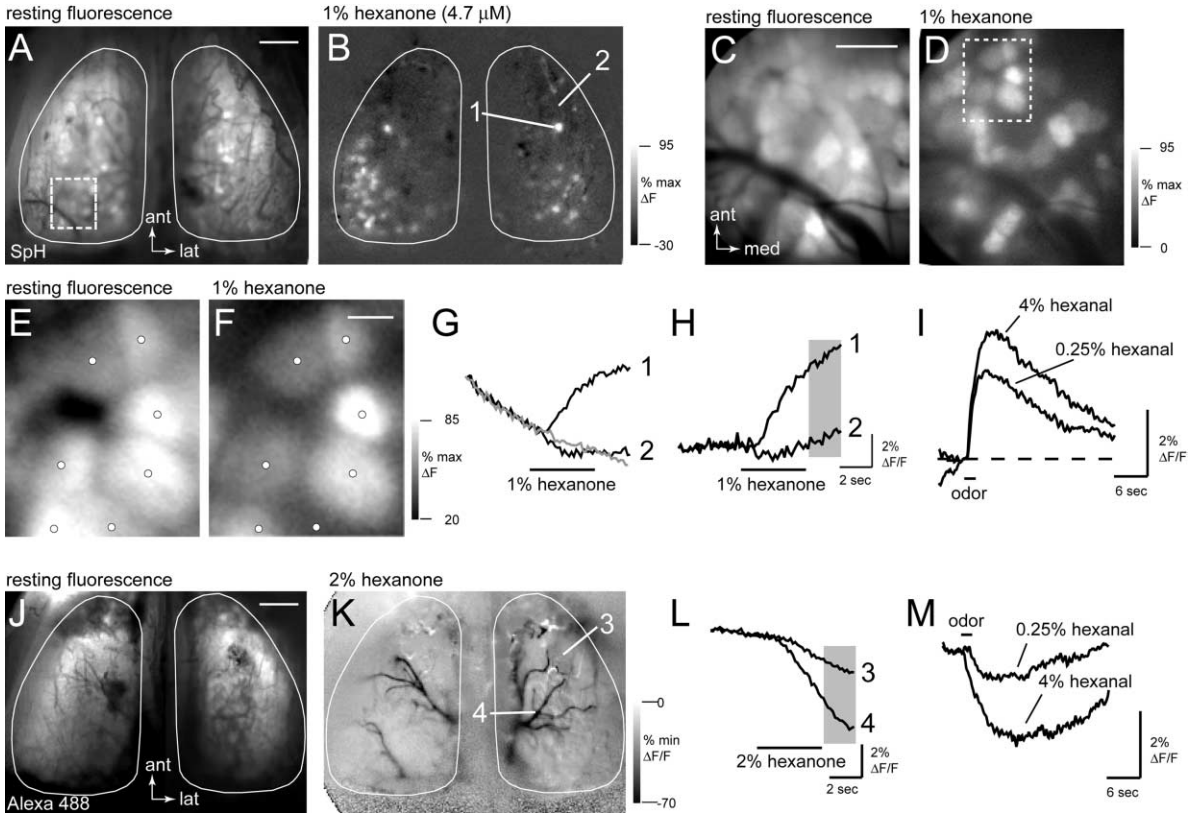

Figure 2. Odorant-Evoked SpH Signals in the Mouse Olfactory Bulb

(A) Resting spH fluorescence in the dorsal olfactory bulbs viewed through thinned bone in a living mouse. Bulb outlines are indicated by white solid lines. Boxed region is shown at higher magnification in panel (C). Anterior (ant) and lateral (lat) are indicated. Scale bar, 500 μm.

(B) Spatial map of the spH signal (ΔF) elicited by 2-hexanone (single trial), showing responses in distinct glomeruli (1). Two regions from which the traces in panels (G) and (H) were derived are indicated (1 and 2). The response map is scaled from 95% to –30% of the maximal ΔF.

(C) Higher magnification of resting fluorescence showing glomeruli (round profiles). Anterior (ant) and medial (med) are indicated. Scale bar, 200 μm.

(D) Odorant-evoked response map from the area in panel (C), showing distinct activated glomeruli. Boxed region is enlarged in panel (F). The map is scaled from 95% to 0% of the maximum ΔF.

(E) High-magnification resting fluorescence image from region marked in panel (D). The centers of presumed individual glomeruli are shown by dots.

(F) Odorant-evoked response map from the same area as in panel (E), showing the profiles of responsive glomeruli. Positions of the dots are the same as in panel (E). Scale bar, 50 μm.

(G) Time course of the fluorescence decrease due to photobleaching (gray trace) taken from a no-stimulus trial, superimposed on the raw traces from two glomeruli (black traces) during a hexanone trial.

(H) Time course of the odorant-evoked spH signal from a hexanone responsive (1) and nonresponsive (2) glomerulus after correction for photobleaching (subtraction of gray trace from panel [G]). Gray box demarcates the image frames used to create the map in panel (B). Data were collected at 7 Hz and presented with no temporal filtering.

(I) Time course of the spH signal from a single glomerulus elicited by two concentrations of hexanal (different preparation than in [A]–[H]). Response to a 2 s stimulus did not fully recover during the 25 s acquisition time. Data were collected at 7 Hz and filtered with a low-pass Gaussian at 1 Hz.

(J) Resting fluorescence in the dorsal olfactory bulbs of a living mouse loaded with Alexa Fluor 488 dextran. Outlines of the bulbs are indicated by white solid line. Scale bar, 500 μm.

(K) Intrinsic optical signal evoked by hexanone (2% s.v.) reveals a strong decrease in fluorescence associated with blood vessels (seen as dark lines) and a smaller, spatially diffuse fluorescence decrease which is difficult to distinguish in the map. Fluorescence decreases from two locations are plotted in panel (L). The image is scaled from 0% to −70% of the maximum ΔF/F.

(L) Odorant-evoked intrinsic signal measured from the regions shown in panel (K). The signal appears as a slow fluorescence decrease (black traces) which is larger in amplitude over blood vessels (4).

(M) Time course of the intrinsic signal elicited by 2 s pulses of two concentrations of hexanal. The amplitude was concentration dependent and showed a similar time course to the spH signal (compare with panel [I]).

cient to nearly offset the decline in fluorescence that occurred during a 10 s trial. In contrast, glomeruli loaded with Oregon Green 488 BAPTA-1 dextran failed to exhibit such a recovery (data not shown, but see Wachowiak and Cohen 2001). Thus, resting fluorescence was reduced by only 11.7% ± 2.4% after 1–3 hr of experimentation (29 glomeruli in three preparations; total illumination time 5–7 min), and images measured at the beginning and end of each experiment were highly correlated ($r = 0.94$, $df = 27$, $p < 0.001$).

The rise time of the glomerular spH signal was slow (Figure 2H), and spH fluorescence increased during prolonged odorant presentations. The spH signal evoked by suprathreshold odorant concentrations (1%–4% saturated vapor [s.v.], hexanal or 2-hexanone) reached half-maximal amplitude at 1.4 ± 0.1 s (n = 26 glomeruli in 3 mice) after stimulus onset for short (2 s) presentation and 2.5 ± 0.2 s (n = 29 glomeruli in 4 mice) for 4 s presentations. Signal recovery was also slow (Figure 2I). Responses to a 2 s stimulus did not fully recover 25 s after stimulus offset. The recovery time course likely reflects the relatively slow process of vesicle endocytosis and vesicle reacidification (Sankaranarayanan and Ryan, 2000).

The fractional change in odorant-evoked spH fluorescence averaged 4.0% ± 0.2% ΔF/F for 2 s presentations of 1%–4% s.v. hexanal or hexanone (n = 5 glomeruli with largest response amplitudes from each of 3 mice). Longer stimuli or higher concentrations evoked signals as large as 15% ΔF/F. The signal-to-noise ratio (S/N) of the spH signal was 49 ± 4 (n = top 5 glomeruli from each of 3 mice, 2 s odorant presentations, see Experimental Procedures). Longer odorant presentations (used in most cases, i.e., Figure 2) tended to increase S/N by increasing signal amplitude.

We found no relationship between resting fluorescence and the maximal (i.e., saturating) spH response amplitude ($r = 0.13$, $df = 27$, $p > 0.5$; 27 glomeruli from four preparations), consistent with the notion that two distinct pools of spH protein, membrane-associated and vesicular, give rise to the resting fluorescence and the signal, respectively (Sankaranarayanan and Ryan, 2000). Thus, we did not normalize by resting fluorescence when constructing spH response maps; however, doing so did not significantly alter the response patterns (data not shown).

Contribution of Intrinsic Signals to SpH Response Maps

To evaluate the contribution of intrinsic signals to spH response maps, we imaged responses from wild-type mice in which OSNs were loaded with the green fluorescent marker Alexa Fluor 488 dextran (Figure 2J). Odorants did not evoke fluorescence increases in Alexa Fluor 488-loaded mice but did elicit slow, spatially diffuse fluorescence *decreases* that were detectable across the entire dorsal bulb (n = 4 bulbs from 3 mice). The signals were particularly strong over blood vessels but did not exhibit foci that might correspond to glomeruli (Figure 2K). Maps of intrinsic signal responses evoked by different odorants were indistinguishable (hexanone and hexanal, 4 bulbs from 3 mice; data not shown). The characteristics of the intrinsic signal are thus quite different from those observed using reflected light at longer wavelengths (Rubin and Katz, 1999; Meister and Bonhoeffer, 2001; Wachowiak and Cohen, 2003).

The intrinsic fluorescence decrease was slow and long lasting (Figures 2L and 2M), increased in amplitude with odorant concentration (Figure 2M), and was slightly smaller than the spH signal: for 2 s odorant presentations, the mean intrinsic signal amplitude was −0.6% ± 0.1% ΔF/F for low odorant concentrations (0.25%–0.5% s.v.; n = 4 bulbs, 3 animals) and −1.7% ± 0.2% ΔF/F for higher concentrations (2%–4% s.v.). The intrinsic signal was also observed in OMP-spH mice (e.g., note the slight fluorescence decrease in trace #2 of Figure 2H). While the intrinsic signal had the potential to distort the time course and absolute amplitude of the spH signal, its diffuse nature prevented it from altering the spatial pattern of spH-mediated glomerular signals.

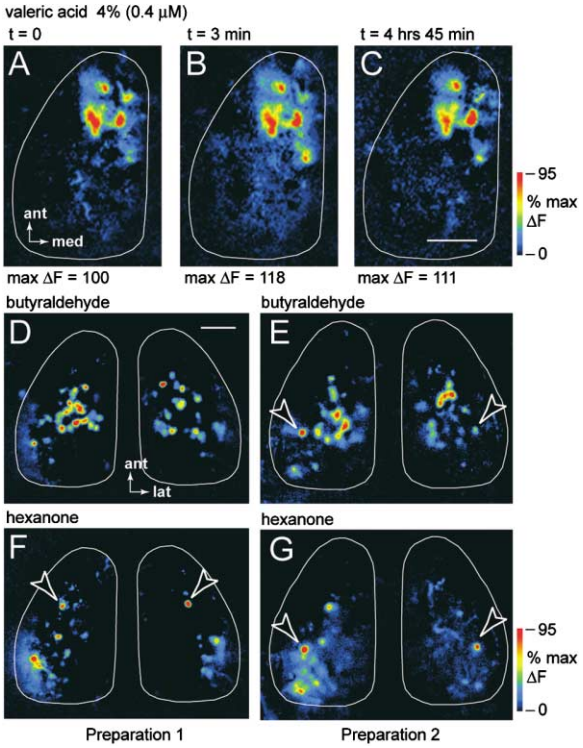

Figure 3. Reproducibility of Odorant-Evoked SpH Signals

(A–C) Response maps from the same mouse evoked during single trials with 4% s.v. valeric acid recorded at three different time points, indicated above each map. The spatial pattern and maximum ΔF observed for each trial (given below each panel in arbitrary units) were similar. Anterior (ant) and medial (med) are indicated. Scale bar, 500 μm.

(D–G) Bilateral response maps from two mice evoked by butyraldehyde (D and E) and 2-hexanone (F and G). Spatial patterns were distinct for different odorants in the same mouse (compare [D] and [F]) but were similar using the same odorant in different mice (compare [D] and [E]). Spatial patterns exhibited some degree of bilateral symmetry. Examples of glomeruli that could be putatively paired in the left and right bulbs are indicated with arrowheads. Concentrations were 1% for (D) and (G), 0.5% for (E), and 1.8% for (F). Scale bar, 500 μm.

Reproducibility of Activity Maps Using SpH

SpH responses were consistent over time. Repeated stimulus presentations over several hours resulted in response maps with similar amplitudes and spatial patterns (Figures 3A–3C). Previous studies indicate that odorant response patterns should be roughly bilaterally symmetric and reproducible across animals (Mombaerts, 1999; Belluscio and Katz, 2001; Meister and Bonhoeffer, 2001). Indeed, both of these features were observed in OMP-spH mice. As examples, Figures 3D–3G show responses from two different mice tested with

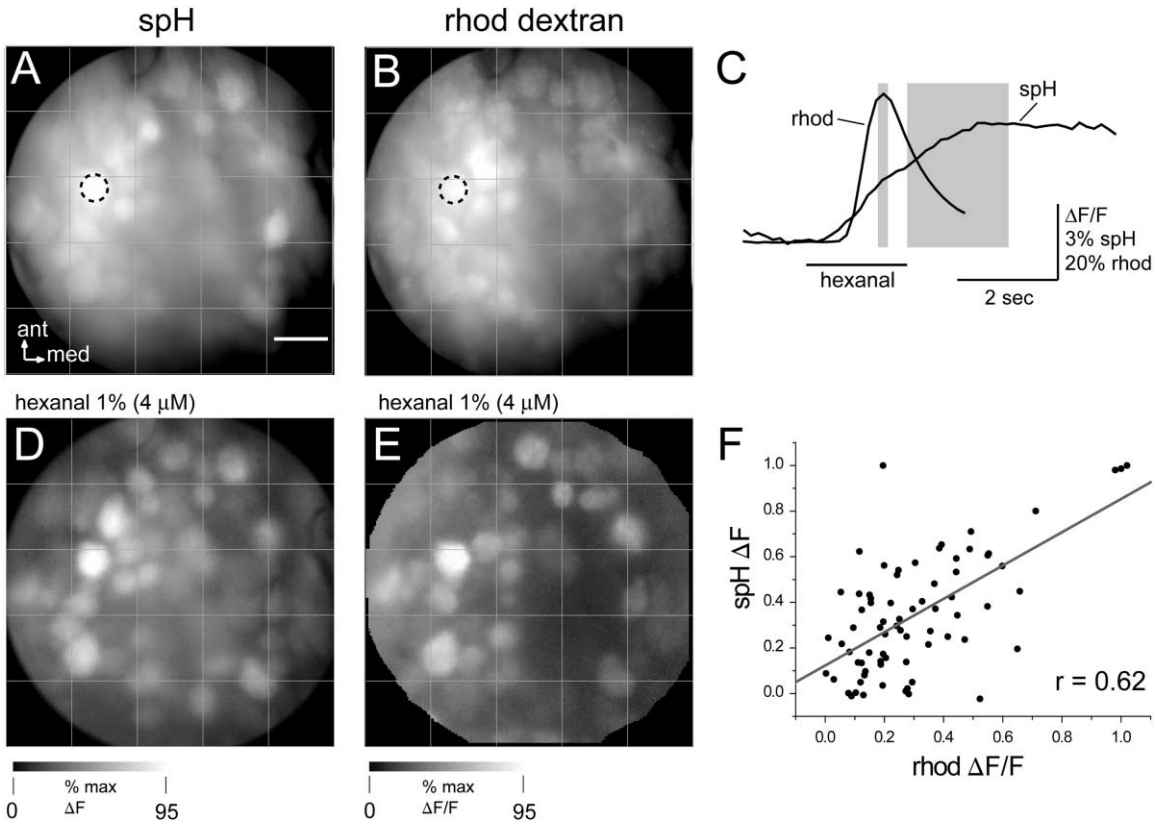

Figure 4. Comparison of SpH and Presynaptic Calcium Signals in Olfactory Bulb Glomeruli

(A and B) Resting fluorescence images of spH (A) and rhod dextran (B) taken from the same olfactory bulb. The overlying grid registers the two images. Circles indicate the glomerulus from which data in panel (C) are derived. Scale bar, 100 μm.

(C) Time course of spH signal (spH) and rhod dextran signal (rhod) from the same glomerulus evoked by a 2 s pulse of hexanal. Shaded areas indicate the temporal windows from which the response maps in panels (D) (spH) and (E) (rhod dextran) were generated. The preparation with the largest rhod dextran signals and typical spH signals was chosen for display. This preparation also exhibited exceptionally strong glomerular labeling with rhod dextran.

(D) Response map using spH, measured as raw change in fluorescence (ΔF). This panel and panel (E) show response maps in grayscale to facilitate comparison of responses at all amplitudes.

(E) Response map using rhod dextran measured as fractional change in fluorescence (ΔF/F).

(F) Correlation between the amplitudes of the spH and rhod dextran responses in rhod-labeled glomeruli, collected from three preparations. Responses were normalized to the maximal signal amplitude in each preparation before performing the correlation. The correlation coefficient is 0.62.

butyraldehyde and hexanone (a similar hexanone response map from a third animal is shown in Figure 2B). Maps were odorant specific, similar for the same odorant across preparations, and roughly bilaterally symmetric within a mouse. For each odorant, several likely homologous glomeruli are apparent in both left and right bulbs and in different mice (Figures 3D–3G). Thus, spH reports patterns of OSN activity in a manner that appears consistent over time and across mice.

Comparison with Presynaptic Calcium Signals

To compare spH signals with an independent measure of odorant-evoked activity, we loaded OSNs of OMP-spH mice with the long-wavelength, calcium-sensitive dye rhod dextran. Because rhod dextran has a relatively low affinity for calcium ($K_d \sim 750$ nM), we reasoned that it would not significantly perturb synaptic vesicle exocytosis. Indeed, there was no difference in time to half-maximal amplitude of the spH signal in the rhod dextran-loaded mice as compared to unloaded mice (rhod-loaded: 1.5 ± 0.1 s, n = 38 glomeruli; unloaded: 1.5 ± 0.1 s, n = 26; t test, df = 62, p = 0.73). Moreover, spH signal amplitude was indistinguishable in rhod-loaded (3.9% ± 0.2% ΔF/F, n = 15 glomeruli) versus nonloaded (4.0% ± 0.2% ΔF/F, n = 15) preparations. Thus, rhod dextran-loading did not perturb odorant responsiveness or presynaptic vesicle release.

The resting fluorescence and S/N ratio of the rhod signal was variable across preparations, presumably due to differences in the effectiveness of dye loading. In addition, the amplitude of the rhod signal diminished rapidly and disappeared after a few trials (data not shown), although spH signals were unaffected. This precluded testing many different odorants or concentrations. Nevertheless, meaningful comparisons of spH and presynaptic calcium signals were made in three mice.

Figure 4 shows the results from one preparation with the strongest rhod signals and typical spH signals. Resting fluorescence images of rhod-loaded and OMP-spH mice were similar (Figures 4A and 4B). Rhod showed

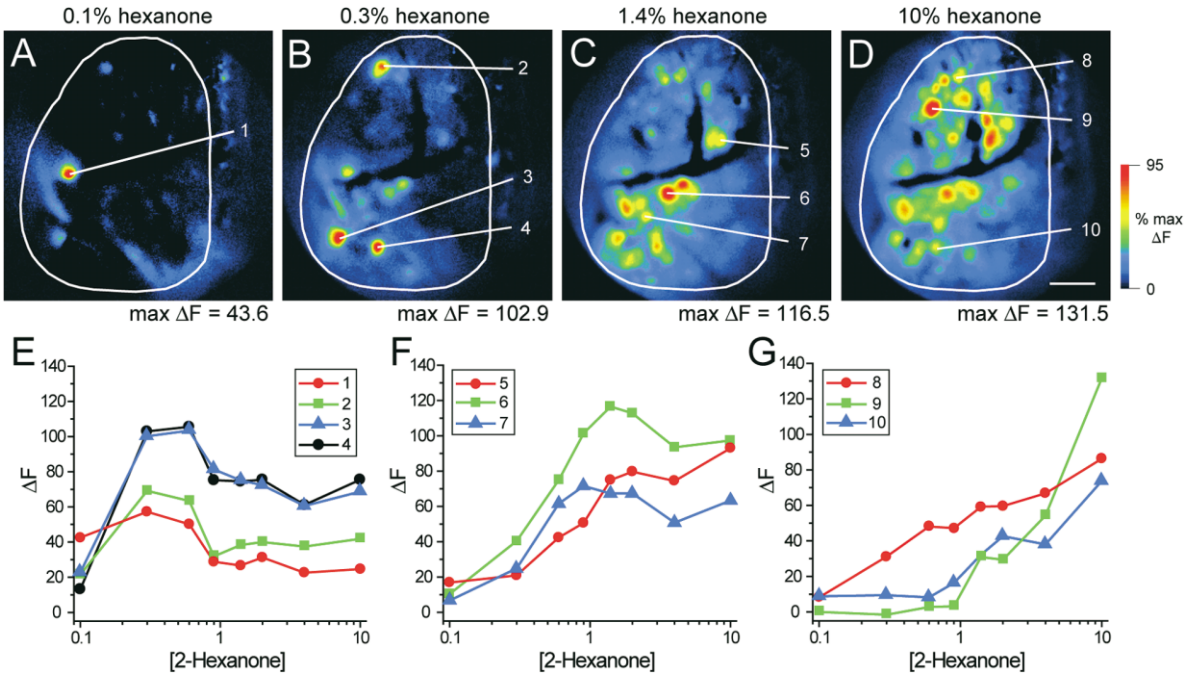

Figure 5. Dynamic Range of SpH Responses in Individual Glomeruli

(A–D) Odorant-response maps elicited with increasing concentrations of 2-hexanone showing recruitment of activated glomeruli with increasing concentration. Percent dilutions of saturated vapor are given in each panel. Glomeruli from which dose-response relationships were plotted are indicated (1 through 10). Because each panel is scaled to its own maximum ΔF (given below each panel), some glomeruli appear to "drop out" of the maps as concentration increases despite their still being activated. Scale bar, 300 μm.

(E) Concentration-response relationships plotted for four glomeruli that exhibited saturation at an intermediate concentration and response decreases at higher concentrations. These were the four glomeruli most sensitive to 2-hexanone in this preparation.

(F) Concentration-response relationships plotted for three glomeruli that exhibited saturating concentration-response relationships.

(G) Concentration-response relationships plotted for three glomeruli that showed no saturation within the concentration range tested.

faster rise times than spH, with responses peaking 1.35 ± 0.04 s after odor onset (n = 30 glomeruli in 3 preparations). Recovery of the rhod signal was also much faster than that of the spH signal. In the two preparations tested with low odorant concentrations, glomerular spH signals appeared at lower concentrations than rhod signals; this effect is presumably due to the relatively low affinity of rhod dextran.

At suprathreshold concentrations, there was a high correspondence between glomeruli showing rhod dextran and spH signals. Figures 4D and 4E show responses to hexanal (1% s.v.) mapped with both indicators. Of 23 glomeruli showing a rhod signal, 22 showed a spH signal. Averaged across all three preparations, 53 of 63 glomeruli (84%) showing rhod signals also showed spH signals, while 53 of 77 (68%) glomeruli showing spH signals also showed rhod dextran signals. The latter disparity may result from the lower rhod dextran sensitivity or incomplete dye loading. Nevertheless, the correspondence between glomeruli showing presynaptic calcium influx and spH signals confirms that spH reports OSN input to glomeruli.

While glomeruli with the strongest rhod signals also showed strong spH signals, spH and rhod response amplitudes (measured from glomeruli showing visible rhod resting fluorescence) were only moderately correlated (Figure 4F; $r = 0.62$, $df = 71$, $p < 0.0001$). This lack of correlation may reflect nonlinearities in the relationship between presynaptic calcium influx and transmitter release (Zucker and Regehr, 2002). In addition, rapid endocytosis and reacidification of presynaptic vesicles (Gandhi and Stevens, 2003) could reduce the spH signal below that predicted by measures of calcium influx.

Sensitivity and Dynamic Range of Stimulus-Evoked SpH Signals

Glomeruli responded to odorant concentrations as low as 0.05%–0.1% s.v. (Figure 5A), the lowest concentrations we could reliably deliver. This sensitivity is comparable to that measured with presynaptic calcium imaging (Wachowiak and Cohen, 2001). Increasing concentration recruited signals from additional glomeruli (Figures 5A–5D). To assess the dynamic range of spH as an indicator of stimulus intensity, we plotted concentration-response relationships for 46 glomeruli (five preparations) in which 2-hexanone or butyraldehyde were presented over a 20- to 100-fold concentration range. Eleven glomeruli (24%) exhibited large responses at the lowest concentrations tested and were excluded from the analysis; seven of these exhibited no increase in response amplitude at higher concentrations (data not shown). The remaining glomeruli showed two general types of concentration-response functions. The first type (19/46, 41%) progressed from no response to a saturated response within the ~2 log unit range of our

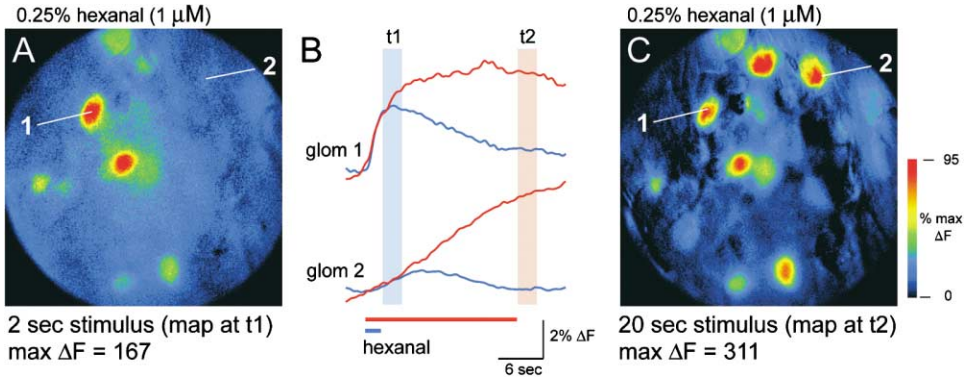

Figure 6. Integration of Neural Activity with SpH

(A) Response map evoked by a single 2 s presentation of a near-threshold concentration of hexanal (0.25% s.v.). Two glomeruli show strong activation. The locations of a single, highly responsive glomerulus (1) and a single weakly responsive glomerulus (2) are indicated.

(B) Time course of spH signals in the indicated glomeruli evoked by 2 s (top) and 20 s (bottom) pulses of hexanal (0.25% s.v.). Glomerulus 2 shows a small, slow response with 2 s stimulation but a continuous increase in signal amplitude with longer stimulation. The shaded regions indicate frames used to derive response maps following the short (t1, blue) and long (t2, red) stimulus applications.

(C) Response map evoked by a 20 s hexanal stimulation. Glomerulus 2 as well as several additional glomeruli that were weakly activated in (A) now show clear spH signals. The absolute magnitude of the spH signal is also larger after 20 s than after 2 s (max ΔF given below the maps).

olfactometer (Figure 5F). For these glomeruli, dynamic range was estimated by fitting the concentration-response plots to a Hill function (Meister and Bonhoeffer 2001; Wachowiak and Cohen 2001). Hill coefficients ranged from 1.28 to 7.28, roughly corresponding to a dynamic range of 0.5 to 1.3 log concentration units. The second type (16/46, 35%) did not saturate at the highest concentrations tested (Figure 5G); half of these (8/16) exhibited a slight response at the lowest concentrations, implying a dynamic range larger than 1.3–2 log units. Thus, the dynamic range of the spH signal was variable across glomeruli but could be as large as or greater than 2 log units.

Some glomeruli (8/46, 17%) showed decreases in spH signal amplitude as concentration increased above the saturating point (see glomeruli 1–4, 6, and 7 in Figures 5E and 5F). This decrease was independent of the time window used to measure signal amplitude (data not shown) and was also observed after background subtraction to correct for potential intrinsic signals. Thus, the relationship between concentration and OSN input to glomeruli could be nonmonotonic. Such an effect may reflect rapid adaptation of OSNs at high concentrations (Duchamp-Viret et al., 2000; Reisert and Matthews, 2001), presynaptic inhibition at the OSN axon terminal (Aroniadou-Anderjaska et al., 2000; Wachowiak and Cohen, 1999), or depression of transmitter release during high-frequency action potential trains (Zucker and Regehr, 2002).

Integrative Nature of the SpH Signal

One potential advantage of the slow recovery of the spH signal is that it may serve as an integrator of presynaptic activity. This feature could be useful for detecting low levels of neuronal activity. We therefore compared response maps obtained with short versus long odorant stimulations using near-threshold concentrations. For the example in Figure 6, a 2 s presentation of hexanal (0.25% s.v.) elicited responses in approximately eight glomeruli (Figure 6A). Weakly activated glomeruli showed a slow, continuous increase in spH signal for the duration of longer odorant presentations, while more strongly activated glomeruli reached a plateau after several seconds (Figure 6B). As a result, a 20 s presentation of hexanal elicited responses in several glomeruli that were not apparent in the maps derived from the short presentation (Figure 6C). In addition, signal amplitudes were higher for the activated glomeruli after the 20 s odorant presentation (Figure 6C) improving the S/N ratio. Thus, by integrating low levels of activity, spH can report neuronal responses that could be below the level of detection of other protein- or chemical-based indicators.

Chronic Imaging of SpH Responses

Persistent expression of genetically encoded probes potentially permits repeated measurements in the same subject over long time periods. We compared odorant response maps from three OMP-spH mice repeatedly imaged over periods ranging from 24 hr to 7 days. Both resting fluorescence and response maps for different odorants were consistent across imaging sessions (Figure 7). Of the 33 glomeruli that responded in the top sixtieth percentile of the signal range during the initial session, 76% responded to the same odorant during subsequent imaging sessions. Failure to detect responses in the other 24% may have arisen from differences in focal plane and head orientation. Thus, spH expression is stable enough to be used in studies requiring longer-term measurements, for instance, in combination with behavioral training or during development.

Topography of Responses with Carbon Chain Length

A standing issue in odor coding is the relationship between odorant structure and spatial patterns of glomerular activity in the bulb (chemotopy). As spH reports OSN input to individual glomeruli with high spatial resolution, we addressed the issue of fine chemotopic mapping of carbon chain length using OMP-spH mice. We examined

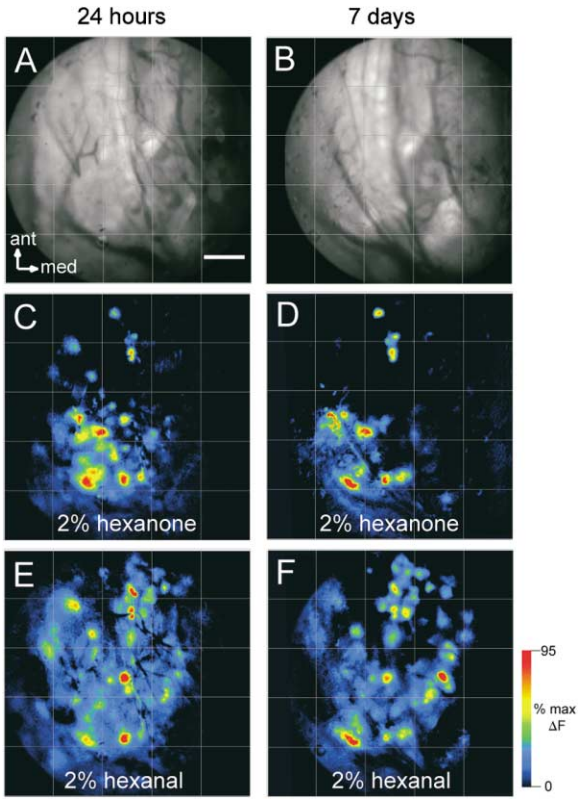

Figure 7. Chronic Imaging of Odorant Representations Using SpH

(A and B) Resting spH fluorescence images in the same mouse taken 24 hr (A) and 7 days (B) after implantation of a chronic imaging chamber. Blood vessels can be seen overlying the glomerular fluorescence. Anterior (ant) and medial (med) are indicated. Scale bar, 300 μm.

(C and D) Response maps to hexanone (2% s.v.) measured at 24 hr (C) and at 7 days (D) are similar.

(E and F) Response maps to hexanal (2% s.v.) also exhibit similar response patterns at 24 hr (E) and 7 days (F). Grid overlays register the images.

response patterns to a homologous series of aliphatic aldehydes with carbon chain lengths ranging from 4 to 8 and a series of aliphatic acids with chain lengths ranging from 3 to 7. We used two strategies. First, we mapped the most sensitive glomeruli by presenting odorants at near-threshold concentrations (Figures 8A and 8B). Mapping was performed in four bulbs from three mice for the aldehydes and three bulbs from three mice for the acids. Near-threshold concentrations evoked strong spH signals in two to ten glomeruli (Figures 8A and 8B). For shorter chain lengths (3–6 carbons), the most sensitive glomeruli localized to the anterior-medial quadrant of the bulb, consistent with previous reports (Uchida et al., 2000; Belluscio and Katz, 2001; Johnson and Leon, 2000). Many glomeruli were maximally sensitive to two adjacent molecules in the homologous series (Zhao et al., 1998; Meister and Bonhoeffer, 2001; Wachowiak and Cohen, 2001; Bozza et al., 2002). Other glomeruli were more broadly tuned (rightmost panels in Figures 8A–8C). For both aldehydes and acids, the most sensitive glomeruli were more broadly distributed with increasing carbon chain length, as has been reported with 2-deoxyglucose mapping (Johnson and Leon, 2000).

We failed to observe any systematic progression of the locations of maximally sensitive glomeruli across a homologous series. While longer chain length odorants (C6–C8) tended to activate more anterior glomeruli, these odorants also activated more caudal and lateral glomeruli (Figures 8A and 8B). Overlays of the most sensitive aldehyde-responsive glomeruli mapped across preparations (see Experimental Procedures) revealed scattered distributions whose centroids did not shift systematically with carbon chain length (Figure 8D). This observation was true for both aldehydes and acids.

We also mapped responses to aldehydes presented at a fixed dilution of saturated vapor, a strategy used in recent intrinsic imaging studies (Uchida et al., 2000; Belluscio and Katz, 2001). Because vapor pressure decreases with increasing chain length, constant vapor dilutions produce molar concentrations that vary over two orders of magnitude across the homologous series. This concentration change could itself produce spatially distinct response patterns (e.g., Figure 5). For 1% dilutions of the aldehyde series, activated glomeruli were scattered across much of the dorsal bulb (Figure 8C). The region showing the highest density of activated glomeruli appeared to move anterior with increasing carbon chain length (Figure 8E), yet the centroid of the distribution of these glomeruli moved only slightly ($<$400 μm) anterior. Thus, the concentration dependence of OSN input to glomeruli may partially account for shifts in the distribution of glomeruli activated across a homologous series.

Discussion

Genetically encoded probes promise to revolutionize functional imaging in the nervous system. However, their use in vivo has been limited, particularly in mammals. Our experiments characterize the use of a particular genetically encoded probe, synapto-pHluorin (Miesenböck et al., 1998), which reports presynaptic vesicle fusion and transmitter release, to measure neuronal activity in living mice. When expressed in OSNs, spH gave rise to odorant-evoked fluorescence increases that were localized to afferent presynaptic terminals in glomeruli of the olfactory bulb. SpH signals were easily detected in living mice and corresponded to independent measurements of calcium influx into OSN presynaptic terminals. The signal amplitudes and signal-to-noise ratios were comparable to those exhibited by conventional calcium-sensitive dyes imaged under the same conditions (Wachowiak and Cohen, 2001). SpH exhibited a dynamic range and sensitivity comparable to those seen with presynaptic calcium imaging. Thus, expression of spH in mammalian neurons can be used to monitor the spatial distribution and relative magnitude of the synaptic output of defined neuronal populations in vivo.

SpH as a Reporter of Neuronal Activity

OMP-driven expression of spH in OSNs may provide a near-ideal situation for imaging neuronal activity in vivo: thousands of functionally similar afferents converge onto an anatomically defined unit (a glomerulus), and

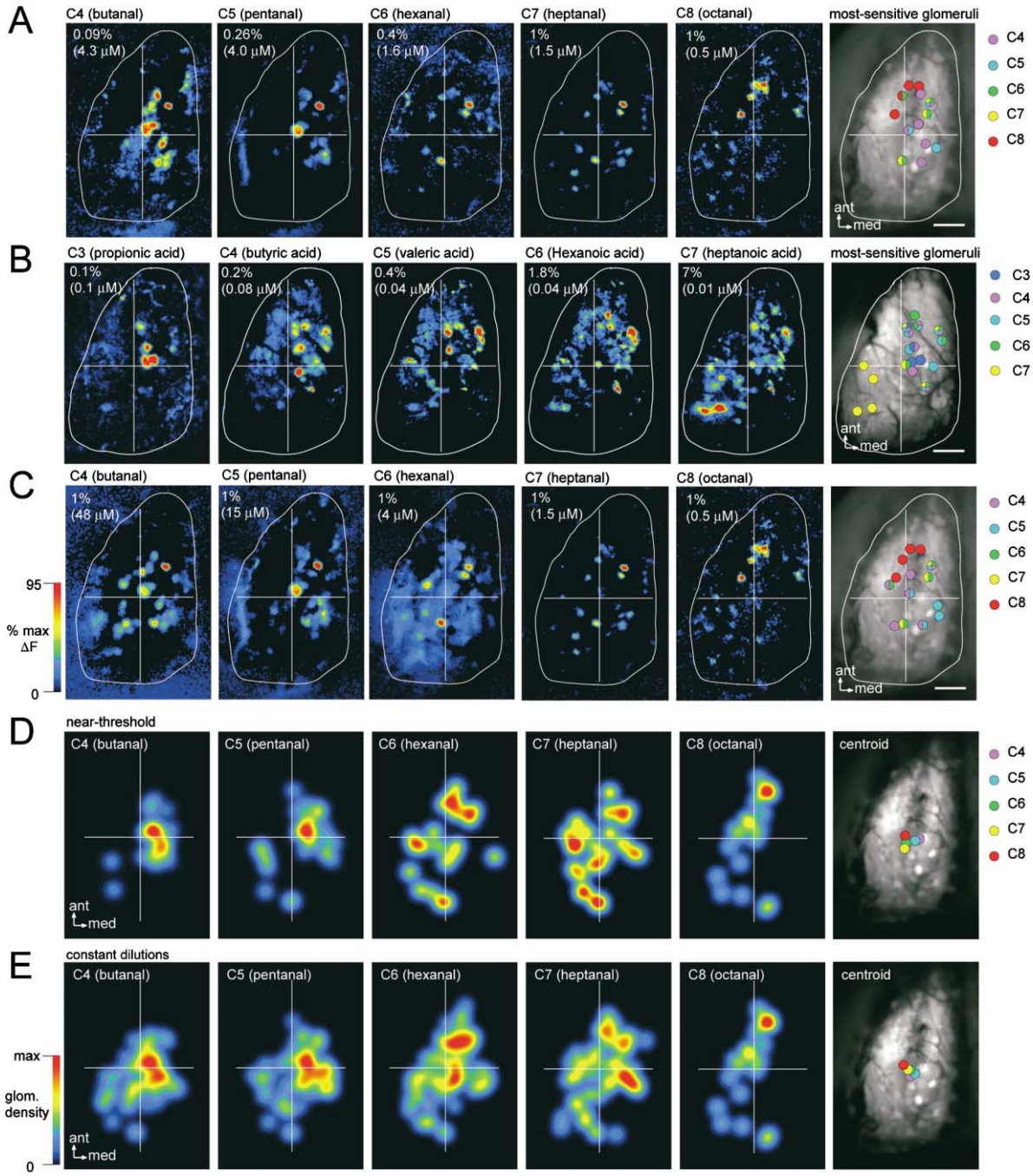

Figure 8. Mapping Responses to a Homologous Odorant Series

(A) Response maps evoked by a homologous series of aliphatic aldehydes (C4 through C8) from a single mouse using near-threshold concentrations. Outline of the olfactory bulb is shown in white. Images are overlaid with a cross to facilitate comparison. The rightmost panel shows the resting fluorescence image overlaid with circles marking the positions of glomeruli with spH signals greater than 40% of the maximum, with each circle color coded by chain length. Reducing the odorant concentration by 50% resulted in little or no response. Scale bar, 500 μm.

(B) Response maps from one mouse using a homologous series of organic acids (C3 through C7) obtained at near-threshold concentrations. Rightmost panel shows the positions of the most sensitive glomeruli responding to each of the six acids, mapped and color coded by chain length as in (A).

(C) Response maps from a single mouse for the aldehyde series presented at a constant 1% dilution of saturated vapor. Note the large change in molar vapor concentration (given in μM) with carbon chain length. The rightmost panel shows overlays of the most strongly activated glomeruli as in (A). Data are from the same mouse as in (A). Maps using heptanal and octanal are the same in (A) and (C) because the near-threshold concentration and constant-vapor concentrations were the same.

(D) Distribution of the most sensitive glomeruli in all four preparations using the near-threshold aldehyde series. Maps were overlaid and positions of the most strongly activated glomeruli marked with a spot (see Experimental Procedures). The spot maps were averaged and smoothed to show the aggregate relative density of activated glomeruli. Right panel shows the corresponding centroids of the summary overlays for each of the aldehydes, color coded as in (A). There is no clear relationship between the distribution of activated glomeruli and carbon chain length.

(E) Summary of the distribution of glomeruli activated by a constant vapor dilution (0.5%, n = 1; 1%, n = 3), as described in (D). The map of glomeruli activated by octanal is the same in (D) and (E) because the near-threshold concentration and constant-vapor concentrations were the same. The panel on the right shows the centroids of the glomerular distributions for each of the aldehydes in the series.

the OMP locus provides unusually high levels of protein expression. What is the likelihood that spH will be successful in reporting activity in other parts of the mammalian nervous system? SpH reports activity in *Drosophila* olfactory glomeruli (Ng et al., 2002) (which encompass many fewer neuronal elements than in mouse) and at single synapses both in vivo (Poskanzer et al., 2003) and in cultured neurons (Miesenböck et al., 1998; Sankaranarayanan et al., 2000; Gandhi and Stevens, 2003). Thus, we expect that spH will likely yield useful signals, either in vivo or in slice preparations, when expressed in other regions of the mouse nervous system.

SpH is unique among protein-based indicators in that it provides a measure of synaptic output (synaptic vesicle release) and may be useful for studying synaptic function (e.g., modulation of neurotransmitter release) from defined neuronal populations in vivo or in slices. One potential limitation of spH is its kinetics, particularly the response recovery which is limited by the slow process of endocytosis (Sankaranarayanan and Ryan, 2000). As a result, spH is not appropriate for monitoring the temporal dynamics of population activity in vivo. However, one consequence of the slow recovery kinetics is that the signal can be integrated over a longer time period, improving the signal-to-noise ratio of the measurement. Thus, spH may be useful for imaging under suboptimal conditions, for example, with noisy detectors, using low incident light, or from structures that emit low levels of fluorescence; such conditions might be encountered when imaging from awake behaving animals or during two-photon or confocal microscopy. In addition, the integrative nature of the spH signal should facilitate the detection of low levels of activity by examining responses to prolonged or repeated stimulus presentations. We have demonstrated that presenting odorants for long periods and measuring the integrated spH response can be used to enhance detection of small signals in weakly activated glomeruli.

While spH is clearly capable of reporting graded responses, the precision with which the signal reports neuronal activity remains unclear. We found that the magnitude of the spH and presynaptic calcium signals were only moderately correlated. This lack of correlation may be due in part to errors associated with measuring signals in vivo (i.e., autofluorescence, low resting levels of rhod dextran fluorescence, contamination by intrinsic signals and out-of-focus light). In addition, the relationship between presynaptic activity and neurotransmitter release is complex and temporally dynamic (Zucker and Regehr, 2002). Interpreting spH signal amplitude is also complicated by contributions of fluorescence decreases arising from vesicle endocytosis and intrinsic optical signals. More experiments, for example, using in vitro preparations, are therefore necessary to understand the precise relationship between spH fluorescence and neuronal activity.

Mapping Receptor Input to the Olfactory Bulb

We used OMP-spH mice to investigate the chemotopy of odorant representations. Detailed odorant representations in rodents have been previously characterized using other functional imaging methods: 2-deoxyglucose metabolism (Johnson and Leon, 2000), functional magnetic resonance imaging (Xu et al., 2000), intrinsic signal imaging (Rubin and Katz, 1999; Uchida et al., 2000; Meister and Bonhoeffer, 2001), and presynaptic calcium-sensitive dye imaging (Wachowiak and Cohen, 2001). These methods have demonstrated that odorant representations are conserved across animals, are roughly bilaterally symmetric, and are dependent on both odorant identity and concentration. We observed all of these basic features in OMP-spH mice.

However, we found little evidence for a finely organized mapping of carbon chain length across the bulb surface, as has been reported by 2-deoxyglucose and intrinsic imaging studies (Uchida et al., 2000; Belluscio and Katz, 2001; Meister and Bonhoeffer, 2001; Johnson and Leon, 2000). Instead, glomeruli that were preferentially tuned to aldehydes or acids of different chain lengths were distributed across largely overlapping regions of the bulb. The discrepancy may lie in the nature of the imaging methods, which measure different correlates of neuronal activity and have differing spatial resolutions. 2-deoxyglucose mapping relies on averaging signals across animals, which prevents the localization of single glomeruli and introduces a detection bias toward clusters of glomerular activity. While it is possible to resolve single glomeruli with intrinsic signals, this measurement can require a significant amount of spatial filtering (Meister and Bonhoeffer, 2001), and the relationship between signal foci and single glomeruli is not always clear (Belluscio and Katz, 2001; Wachowiak and Cohen, 2003). We also found that odorant concentration can alter glomerular activation patterns such that mapping a homologous series is confounded by vapor pressure changes associated with carbon chain length. A more speculative explanation is that the intrinsic and 2-deoxyglucose signals primarily reflect postsynaptic activity and that finely organized chemotopy is an emergent property of postsynaptic processing.

Clearly, a more extensive mapping of glomerular responses to related odorants is necessary to fully understand odorant representations at the level of olfactory bulb input. The fidelity with which OSN input to single glomeruli can be mapped using spH should be useful in addressing this issue.

Future Application of SpH in the Olfactory System

We expect that spH can be used to address a number of important questions in olfactory biology. First, spH could be targeted to output neurons (mitral/tufted cells of the olfactory bulb), as has been done in the *Drosophila* olfactory system (Ng et al., 2002), permitting the investigation of odorant representations through multiple synaptic levels. Second, spH could be exploited to record activity in genetically identified glomeruli using mice in which afferents expressing a given odorant receptor are tagged with a spectrally separable fluorescent marker. Third, OMP-spH mice should be valuable in studying the stability of odorant representations during development and potential plasticity during learning (Johnson et al., 1995). The present study demonstrates the feasibility of chronic imaging using OMP-spH mice. Finally, because the OMP locus drives expression of spH in vomeronasal sensory neurons, the OMP-spH strain may permit similar imaging of sensory input to the accessory olfactory bulb,

which is thought to process pheromone-mediated information regarding social and sexual status (Dulac and Torello, 2003). The anatomy of the vomeronasal epithelium and accessory olfactory bulb severely limits dye loading using conventional methods.

General Applicability of Protein-Based Indicators

Few methods are available for high-resolution imaging of neuronal activity in the intact mammalian nervous system. Intrinsic signal and voltage-sensitive dye imaging (Lieke et al., 1989) have provided important insights into the functional organization of the mammalian brain. The development of genetically encoded probes provides the opportunity to image activity specifically from defined neuronal populations in vivo. The success of spH in reporting neuronal activity in the intact mouse is an important step in this development. Further improvements in genetic probes, gene targeting, and optical imaging technologies promise to greatly expand our window into brain function.

Experimental Procedures

Gene Targeting

An expression vector (*pCI*) containing superecliptic spH was provided by Dr. G. Miesenböck. The coding sequence with Kozak consensus was excised as an EcoRI-XbaI fragment and cloned into a polylinker containing an upstream PacI site. An autoexcising *neo* cassette (Bunting et al., 1999) was inserted as an XbaI fragment introducing a downstream PacI site, *ACNF* (Bozza et al., 2002), creating the *SEspH-ACNF* cassette. The cassette was inserted as a PacI fragment into the OMP targeting vector (Mombaerts et al., 1996). The vector was linearized and electroporated into E14 ES cells as described (Mombaerts et al., 1996). Genomic DNA from G418-resistant ES clones was analyzed by Southern blot hybridization with probes external to the targeting vector. Homologous recombinant ES cells were injected into C57BL/6 blastocysts and chimeras were obtained. The autoexcising *neo*-selectable cassette was removed in the germline of chimeras. Transmission of the resulting allele was confirmed by PCR analysis of F1 progeny. The strain used for analysis is derived from ES clone OSE-80 and is of a mixed (129 × C57BL6/J) background. OMP-spH mice will be available from The Jackson Laboratory (Bar Harbor, Maine), stock #4946.

Dye Loading and In Vivo Imaging

OSNs were loaded in vivo with either rhod dextran, 10 kDa MW, "high affinity" or Alexa Fluor 488 dextran, 10 kDa MW (Molecular Probes, Eugene, OR) as previously described (Friedrich and Korsching, 1997; Wachowiak and Cohen, 2001). Mice were held 4–8 days to allow transport of dye to OSN axon terminals.

Imaging was performed in heterozygous (n = 23) and homozygous (n = 5) OMP-spH mice and in 129/B6 mixed-background mice (n = 3), 4–20 weeks of age. Although OMP-spH homozygous mice lack OMP, no obvious differences were observed in the sensitivity or time course of the odorant-evoked responses between heterozygous and homozygous mice. All data analyzed and displayed are from heterozygous mice. Of these, 14 were F1 progeny of crosses to a strain in which the M72 odorant receptor gene is tagged with a fluorescent reporter (data not shown).

In vivo imaging was performed in pentobarbital-anesthetized mice, as described previously (Wachowiak and Cohen, 2001). The olfactory bulbs were imaged through thinned bone using an Olympus BX51WI microscope and epifluorescence condenser, with 4× (0.28 NA), 10× (0.3 NA), or 20× (0.95 NA) Olympus objectives. Illumination was provided by a 150W Xenon arc lamp (Opti-Quip, New York) attenuated with a 25% ND filter. Filter sets were as follows: spH and Alexa Fluor 488, HQ480/40 (exciter), Q505LP (dichroic), HQ535/50 (emitter); rhod dextran, D540/25 (exciter), 555 DCLP (dichroic), D620/60 (emitter). Optical signals were recorded using a back-illuminated CCD camera (NeuroCCD, SM-256, RedShirtImaging, Fairfield, CT) at 256 × 256 pixel resolution and a frame rate of 7 Hz or at 128 × 128 pixel resolution at a frame rate of 125 Hz. Data acquisition was performed with Neuroplex software (RedShirtImaging, Fairfield, CT).

Odorant Presentation

Odorants (95%–99% pure) were obtained from Sigma or Fluka and were diluted from saturated vapor in cleaned, desiccated air using a mass flow controller (Aalborg, Orangeburg, NY). Nitrogen was used as the vapor carrier to avoid oxidation. Separate lines for each odorant avoided cross-contamination. Concentrations are expressed as percent dilutions of saturated vapor and as molar vapor concentrations, estimated from Yaws (1994). The olfactometer followed the design of Kauer and Moulton (1974) and Lam et al. (2000) and delivered square pulses at a flow rate of 300–500 ml/min. Pulse duration ranged from 2–20 s, typically 2 or 4 s. The interstimulus interval was at least 60 s. Repeated stimulus presentation at this interstimulus interval evoked similar response amplitudes. In most mice (n = 22), a double tracheotomy was performed and odorants presented using a 3 Hz artificial sniff protocol (Wachowiak and Cohen, 2001). Odorant onset and sniff cycle were time locked across trials for multitrial averaging. Odorant-evoked responses were more sensitive and more consistent using the artificial sniff.

Chronic Imaging

The bone overlying the dorsal bulbs was thinned and the surface coated with clear-drying cyanoacrylate (Loctite #41145, Rocky Hill, CT). Mice were fitted with acrylic head caps fastened to the skull with acrylic and bone screws. Anesthetized mice were secured by bolts connecting the headholder to nuts in the head cap. Mice were imaged immediately after surgery and at one or more time points up to 7 days later.

Data Analysis

Raw traces were corrected for photobleaching by subtracting "no odor" trials before further analysis. Maps of spH signal amplitude were constructed by subtracting the temporal average of a 2 s time window just preceding stimulus onset from a 2 s temporal average beginning just after odorant offset. For display, most response maps were clipped at a minimum of zero and a maximum of 95% of the maximal signal amplitude (ΔF) for that map. In some figures, pixelation was avoided by doubling the pixel resolution and interpolating between pixels. No additional spatial filtering was performed.

Widths of spH signal foci were measured from response maps by fitting the signal intensity profile through a glomerulus with a Gaussian function (Wachowiak and Cohen, 2001). Glomerular diameters and half-widths were calculated from the sigma of the fitted Gaussian (Meister and Bonhoeffer, 2001). SpH signal amplitudes were measured by spatially averaging pixels overlying the glomerulus of interest. Absolute response amplitude (used in all analyses) was measured by subtracting the fluorescence values in the prestimulus temporal window from those in the poststimulus temporal window. In some cases, signal amplitudes relative to the adjacent background were measured by taking the height of the Gaussian fit to the glomerular signal intensity profile (see above). Strongly activated glomeruli were identified by visual inspection while weakly activated glomeruli were chosen or rejected as described in Wachowiak and Cohen (2001). Briefly, signal foci were fitted to a Gaussian and counted only if their half-width was within 2 SD of the mean measured from 52 test glomeruli, and their amplitude was >8 times the root-mean-square spatial noise measured from adjacent nonactivated areas.

S/N ratios were calculated by dividing the absolute response amplitude from an activated glomerulus by the root-mean-square noise measured from the same pixels over the length of a nonstimulus trial. Blank trials were high-pass filtered at 0.5 Hz before the noise measurements to avoid contributions of photobleaching. All S/N measurements were made from single trials.

Resting fluorescence was calculated from the average fluorescence during the first five frames of illumination. For photobleaching analysis, resting fluorescence was averaged across the entire dorsal bulb, which was illuminated with a 10×, 0.3 NA immersion objective

and 25% ND filter. For correlating resting fluorescence intensities with maximal response amplitudes, glomeruli were defined as exhibiting a maximal (saturated) response when a 100% increase in concentration resulted in a less than 25% increase in signal amplitude. Resting fluorescence levels were normalized to the maximum within animals before determining the correlation. Concentration-response functions were plotted using absolute response amplitude measurements (i.e., without background subtraction). Measuring amplitudes relative to background did not affect the observed glomerular dynamic ranges. Hill coefficients were calculated from the best-fit Hill function relating the response amplitude to odorant concentration (Wachowiak and Cohen, 2001). For glomeruli showing decreases in signal amplitude above saturation, V_{max} was constrained to the maximal response amplitude. Dynamic range was computed as the concentration range between 10% and 90% of the maximum of the fitted curve.

For correlating rhod dextran and spH response amplitudes, glomeruli were chosen by appearance in images of rhod resting fluorescence. This criterion excluded glomeruli showing spH signals but no rhod signals but insured that non-rhod loaded glomeruli were excluded from the analysis. This criterion included glomeruli that showed neither spH nor rhod dextran signals. Amplitudes were measured relative to background (see above).

For analysis of the homologous aldehyde and acid series data, glomeruli showing spH signals greater than 30% of the maximal amplitude for a given odorant were represented with a spot. Spot maps were aligned across preparations using the midline and caudal sinus of the bulb as landmarks, and maps for a given carbon chain length averaged. Centroids of activation were calculated from these overlays. In Figures 8D and 8E, the overlays of the spot maps were smoothed with a Gaussian kernel (half-width = 160 μm), normalized and pseudocolored.

Data are expressed as means $\pm$ SEM. Data processing and display were performed with Neuroplex software and with custom software written in IDL, LabVIEW, and MatLab. Curve fits and statistical tests were performed using Origin and StatView.

Histology

SpH fluorescence was observed in unfixed whole mounts. Frozen sections were taken following perfusion with 4% paraformaldehyde. Sections were counterstained with the nuclear dye TOTO-3. Whole mounts and sections were analyzed using a Zeiss LSM 510 confocal microscope. Glomerular areas were measured from flattened confocal stacks taken from approximately the same region of the dorsal bulb from which recordings were made in living mice. Glomerular diameter was taken as $d = 2\sqrt{(\text{area}/\pi)}$ (Meister and Bonhoeffer, 2001). Morphological analysis was done using Zeiss LSM software.

Acknowledgments

This work was supported by grants from the National Institutes of Health. We thank Christina Muratore and Minh-Ha Lieu for assistance with data analysis; Gero Miesenböck for kindly providing the synapto-pHluorin construct; and Paul Feinstein and Tim McClintock for helpful comments on the manuscript.

Received: December 12, 2003
Revised: January 23, 2004
Accepted: February 25, 2004
Published: April 7, 2004

References

Aroniadou-Anderjaska, V., Zhou, F.-M., Priest, C.A., Ennis, M., and Shipley, M.T. (2000). Tonic and synaptically evoked presynaptic inhibition of sensory input to the rat olfactory bulb via GABAB heteroreceptors. J. Neurophysiol. *84*, 1194–1203.

Ataka, K., and Pieribone, V.A. (2002). A genetically targetable fluorescent probe of channel gating with rapid kinetics. Biophys. J. *82*, 509–516.

Baird, G.S., Zacharias, D.A., and Tsien, R.Y. (1999). Circular permutation and receptor insertion within green fluorescent proteins. Proc. Natl. Acad. Sci. USA *96*, 11241–11246.

Belluscio, L., and Katz, L.C. (2001). Symmetry, stereotypy, and topography of odorant representations in mouse olfactory bulbs. J. Neurosci. *21*, 2113–2122.

Bozza, T.C., Feinstein, P.G., Zheng, C., and Mombaerts, P. (2002). Odorant receptor expression defines functional units in the mouse olfactory system. J. Neurosci. *22*, 3033–3043.

Bunting, M., Bernstein, K.E., Greer, J.M., Capecchi, M.R., and Thomas, K.R. (1999). Targeting genes for self-excision in the germ line. Genes Dev. *13*, 1524–1528.

Djurisic, M., Zochowski, M., Wachowiak, M., Falk, C.X., Cohen, L.B., and Zecevic, D. (2003). Optical monitoring of neural activity using voltage-sensitive dyes. Methods Enzymol. *361*, 423–451.

Duchamp-Viret, P., Duchamp, A., and Chaput, M.A. (2000). Peripheral odor coding in the rat and frog: quality and intensity specification. J. Neurosci. *20*, 2383–2390.

Dulac, C., and Torello, A.T. (2003). Molecular detection of pheromone signals in mammals: from genes to behaviour. Nat. Rev. Neurosci. *4*, 551–562.

Fiala, A., Spall, T., Diegelmann, S., Eisermann, B., Sachse, S., Devaud, J.M., Buchner, E., and Galizia, C.G. (2002). Genetically expressed cameleon in *Drosophila melanogaster* is used to visualize olfactory information in projection neurons. Curr. Biol. *12*, 1877–1884.

Friedrich, R.W., and Korsching, S.I. (1997). Combinatorial and chemotopic odorant coding in the zebrafish olfactory bulb visualized by optical imaging. Neuron *18*, 737–752.

Gandhi, S.P., and Stevens, C.F. (2003). Three modes of synaptic vesicular recycling revealed by single-vesicle imaging. Nature *423*, 607–613.

Higashijima, S.I., Masino, M.A., Mandel, G., and Fetcho, J.R. (2003). Imaging neuronal activity during zebrafish behavior with a genetically encoded calcium indicator. J. Neurophysiol. *20*, 3986–3997.

Johnson, B.A., and Leon, M. (2000). Odorant molecular length: one aspect of the olfactory code. J. Comp. Neurol. *426*, 330–338.

Johnson, B.A., Woo, C.C., Duong, H., Nguyen, V., and Leon, M. (1995). A learned odor evokes an enhanced Fos-like glomerular response in the olfactory bulb of young rats. Brain Res. *699*, 192–200.

Kauer, J.S., and Moulton, D.G. (1974). Responses of olfactory bulb neurones to odour stimulation of small nasal areas in the salamander. J. Physiol. *243*, 717–737.

Kerr, R., Lev-Ram, V., Baird, G., Vincent, P., Tsien, R.Y., and Schafer, W.R. (2000). Optical imaging of calcium transients in neurons and pharyngeal muscle of *C. elegans*. Neuron *26*, 583–594.

Kuner, T., and Augustine, G.J. (2000). A genetically encoded ratiometric indicator for chloride: capturing chloride transients in cultured hippocampal neurons. Neuron *27*, 447–459.

Lam, Y.W., Cohen, L.B., Wachowiak, M., and Zochowski, M.R. (2000). Odors elicit three different oscillations in the turtle olfactory bulb. J. Neurosci. *20*, 749–762.

Lieke, E.E., Frostig, R.D., Arieli, A., Ts'o, D.Y., Hildesheim, R., and Grinvald, A. (1989). Optical imaging of cortical activity: real-time imaging using extrinsic dye-signals and high resolution imaging based on slow intrinsic-signals. Annu. Rev. Physiol. *51*, 543–559.

Meister, M., and Bonhoeffer, T. (2001). Tuning and topography in an odor map on the rat olfactory bulb. J. Neurosci. *21*, 1351–1360.

Miesenböck, G., De Angelis, D.A., and Rothman, J.E. (1998). Visualizing secretion and synaptic transmission with pH-sensitive green fluorescent proteins. Nature *394*, 192–195.

Miyawaki, A. (2003). Fluorescence imaging of physiological activity in complex systems using GFP-based probes. Curr. Opin. Neurobiol. *13*, 591–596.

Mombaerts, P. (1999). Seven-transmembrane proteins as odorant and chemosensory receptors. Science *286*, 707–711.

Mombaerts, P., Wang, F., Dulac, C., Chao, S.K., Nemes, A., Mendelsohn, M., Edmondson, J., and Axel, R. (1996). Visualizing an olfactory sensory map. Cell *87*, 675–686.

Nagai, T., Sawano, A., Park, E.S., and Miyawaki, A. (2001). Circularly

permuted green fluorescent proteins engineered to sense Ca^{2+}. Proc. Natl. Acad. Sci. USA *98*, 3197–3202.

Nakai, J., Ohkura, M., and Imoto, K. (2001). A high signal-to-noise Ca(2+) probe composed of a single green fluorescent protein. Nat. Biotechnol. *19*, 137–141.

Ng, M., Roorda, R.D., Lima, S.Q., Zemelman, B.V., Morcillo, P., and Miesenböck, G. (2002). Transmission of olfactory information between three populations of neurons in the antennal lobe of the fly. Neuron *36*, 463–474.

Poskanzer, K.E., Marek, K.W., Sweeney, S.T., and Davis, G.W. (2003). Synaptotagmin I is necessary for compensatory synaptic vesicle endocytosis *in vivo*. Nature *426*, 559–563.

Potter, S.M., Zheng, C., Koos, D.S., Feinstein, P., Fraser, S.E., and Mombaerts, P. (2001). Structure and emergence of specific olfactory glomeruli in the mouse. J. Neurosci. *21*, 9713–9723.

Reisert, J., and Matthews, H.R. (2001). Simultaneous recording of receptor current and intraciliary Ca^{2+} concentration in salamander olfactory receptor cells. J. Physiol. *535*, 637–645.

Romoser, V.A., Hinkle, P.M., and Persechini, A. (1997). Detection in living cells of Ca^{2+}-dependent changes in the fluorescence emission of an indicator composed of two green fluorescent protein variants linked by a calmodulin-binding sequence. A new class of fluorescent indicators. J. Biol. Chem. *272*, 13270–13274.

Rubin, B.D., and Katz, L.C. (1999). Optical imaging of odorant representations in the mammalian olfactory bulb. Neuron *23*, 499–511.

Sakai, R., Repunte-Canonigo, V., Raj, C.D., and Knopfel, T. (2001). Design and characterization of a DNA-encoded, voltage-sensitive fluorescent protein. Eur. J. Neurosci. *13*, 2314–2318.

Sankaranarayanan, S., and Ryan, T.A. (2000). Real-time measurements of vesicle-SNARE recycling in synapses of the central nervous system. Nat. Cell Biol. *2*, 197–204.

Sankaranarayanan, S., De Angelis, D., Rothman, J.E., and Ryan, T.A. (2000). The use of pHluorins for optical measurements of presynaptic activity. Biophys. J. *79*, 2199–2208.

Siegel, M.S., and Isacoff, E.Y. (1997). A genetically encoded optical probe of membrane potential. Neuron *19*, 735–741.

Truong, K., Sawano, A., Mizuno, H., Hama, H., Tong, K.I., Mal, T.K., Miyawaki, A., and Ikura, M. (2001). FRET-based in vivo Ca^{2+} imaging by a new calmodulin-GFP fusion molecule. Nat. Struct. Biol. *8*, 1069–1073.

Uchida, N., Takahashi, Y.K., Tanifuji, M., and Mori, K. (2000). Odor maps in the mammalian olfactory bulb: domain organization and odorant structural features. Nat. Neurosci. *3*, 1035–1043.

Wachowiak, M., and Cohen, L.B. (1999). Presynaptic inhibition of primary olfactory afferents mediated by different mechanisms in lobster and turtle. J. Neurosci. *19*, 8808–8817.

Wachowiak, M., and Cohen, L.B. (2001). Representation of odorants by receptor neuron input to the mouse olfactory bulb. Neuron *32*, 723–735.

Wachowiak, M., and Cohen, L.B. (2003). Correspondence between odorant-evoked patterns of receptor neuron input and intrinsic optical signals in the mouse olfactory bulb. J. Neurophysiol. *89*, 1623–1639.

Wang, J.W., Wong, A.M., Flores, J., Vosshall, L.B., and Axel, R. (2003). Two-photon calcium imaging reveals an odor-evoked map of activity in the fly brain. Cell *112*, 271–282.

Xu, F., Greer, C.A., and Shepherd, G.M. (2000). Odor maps in the olfactory bulb. J. Comp. Neurol. *422*, 489–495.

Yaws, C.L. (1994). Handbook of Vapor Pressure (Houston: Gulf Professional Publishing).

Yu, D., Baird, G.S., Tsien, R.Y., and Davis, R.L. (2003). Detection of calcium transients in *Drosophila* mushroom body neurons with camgaroo reporters. J. Neurosci. *23*, 64–72.

Zhao, H., Ivic, L., Otaki, J.M., Hashimoto, M., Mikoshiba, K., and Firestein, S. (1998). Functional expression of a mammalian odorant receptor. Science *279*, 237–242.

Zucker, R.S., and Regehr, W.G. (2002). Short-term synaptic plasticity. Ann. Rev. Physiol. *64*, 355–405.